



1 **Cluster Dynamics-based Parameterization for Sulfuric Acid-Dimethylamine**
2 **Nucleation: Comparison and Selection through Box- and Three-Dimensional-**
3 **Modeling**

4 Jiewen Shen^{1,2}, Bin Zhao^{1,2}, Shuxiao Wang^{1,2,*}, An Ning³, Yuyang Li², Runlong Cai⁴,
5 Da Gao^{1,2}, Biwu Chu^{5,6}, Yang Gao⁷, Manish Shrivastava⁸, Jingkun Jiang², Xiuhui
6 Zhang³, Hong He^{5,6}

7
8 ¹*State Key Joint Laboratory of Environment Simulation and Pollution Control, School*
9 *of Environment, Tsinghua University, Beijing, 100084, China*

10 ²*State Environmental Protection Key Laboratory of Sources and Control of Air*
11 *Pollution Complex, Beijing, 100084, China*

12 ³*Key Laboratory of Cluster Science, Ministry of Education of China, School of*
13 *Chemistry and Chemical Engineering, Beijing Institute of Technology, Beijing, 100081,*
14 *China*

15 ⁴*Shanghai Key Laboratory of Atmospheric Particle Pollution and Prevention (LAP³),*
16 *Department of Environmental Science & Engineering, Fudan University, Shanghai,*
17 *200438, China*

18 ⁵*State Key Joint Laboratory of Environment Simulation and Pollution Control,*
19 *Research Center for Eco-Environmental Sciences, Chinese Academy of Sciences,*
20 *Beijing 100085, China*

21 ⁶*College of Resources and Environment, University of Chinese Academy of Sciences,*
22 *Beijing 100049, China*

23 ⁷*Key Laboratory of Marine Environment and Ecology, Ministry of Education, Ocean*
24 *University of China, Qingdao 266100, China*

25 ⁸*Pacific Northwest National Laboratory, Richland, Washington, USA*

26

27 *Correspondence to: Shuxiao Wang (shxwang@tsinghua.edu.cn)

28



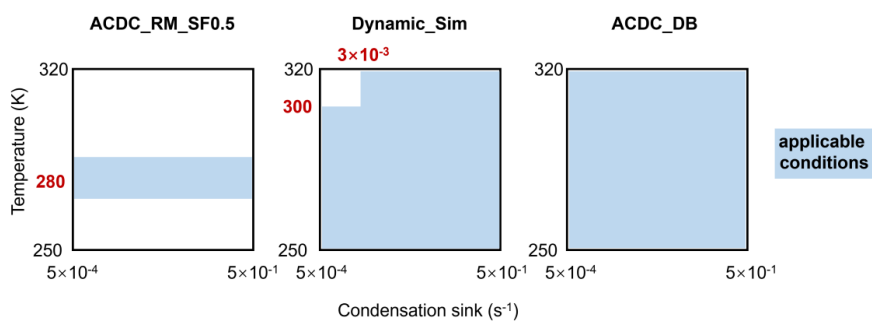
29 **ABSTRACT**

30 Clustering of gaseous sulfuric acid (SA) enhanced by dimethylamine (DMA) is a
31 major mechanism for new particle formation (NPF) in polluted atmospheres. However,
32 uncertainty remains regarding the SA-DMA nucleation parameterization that
33 reasonably represents cluster dynamics and is applicable across various atmospheric
34 conditions. This uncertainty hinders accurate three-dimensional (3-D) modeling of NPF
35 and subsequent assessment of its environmental and climatic impacts. Here we
36 extensively compare different cluster dynamics-based parameterizations for SA-DMA
37 nucleation and identify the most reliable one through a combination of box-model
38 simulations, 3-D modeling, and in-situ observations. Results show that the
39 parameterization derived from Atmospheric Cluster Dynamic Code (ACDC)
40 simulations, incorporating the latest theoretical insights (DLPNO-CCSD(T)/aug-cc-
41 pVTZ// ω B97X-D/6-311++G(3df,3pd) level of theory) and adequate representation of
42 cluster dynamics, exhibits dependable performance in 3-D NPF simulation for both
43 winter and summer conditions in Beijing and shows promise for application in diverse
44 atmospheric conditions. Another ACDC-derived parameterization, replacing the level
45 of theory with RI-CC2/aug-cc-pV(T+d)Z//M06-2X/6-311++G(3df,3pd), also performs
46 well in NPF modeling at relatively low temperatures around 280 K but exhibits
47 limitations at higher temperatures due to inappropriate representation of SA-DMA
48 cluster thermodynamics. Additionally, a previously reported parameterization
49 incorporating simplifications is applicable for simulating NPF in polluted atmospheres
50 but tends to overestimate particle formation rates under conditions of elevated
51 temperature ($> \sim 300$ K) and low condensation sink ($< \sim 3 \times 10^{-3} \text{ s}^{-1}$). Our findings
52 highlight the applicability of the new ACDC-derived parameterization, which couples
53 the latest SA-DMA nucleation theory and holistic cluster dynamics, in 3-D NPF
54 modeling. The ACDC-derived parameterization framework provides valuable reference
55 for developing parameterizations for other nucleation systems.

56



57 **GRAPHICAL ABSTRACT**



ACDC_RM_SF0.5:

ACDC-derived parameterization with traditional theoretical approach

Dynamic_Sim:

reported parameterization with simplifications in cluster dynamics

ACDC_DB:

ACDC-derived parameterization with latest theoretical approach

58

59



60 1 INTRODUCTION

61 Atmospheric aerosols have significant impacts on visibility, human health, and
62 global climate (Gordon et al., 2016). New Particle Formation (NPF) is the predominant
63 source of global aerosol population, with nucleation being the key stage of the gas-to-
64 particle transformation (Zhao et al., 2020; Almeida et al., 2013). In polluted regions
65 such as urban China, compelling evidence indicates that sulfuric acid (SA)-driven
66 nucleation enhanced by dimethylamine (DMA) can generate thermodynamically stable
67 SA-DMA clusters and lead to high particle formation rates close to kinetic limit of SA
68 clustering, which is responsible for the observed intensive NPF events (Cai et al., 2021;
69 Yao et al., 2018). Meanwhile, it has been demonstrated that variations in atmospheric
70 conditions, including condensation sinks (CS) arising from background aerosols, along
71 with temperature (T), can exert profound impacts on the cluster dynamics of SA-DMA
72 nucleation by varying the particle formation rates across several orders of magnitude
73 (Cai et al., 2021; Deng et al., 2020). Given that complex interactions exist among
74 various gaseous precursors, molecular clusters, and pre-existing aerosols during
75 nucleation, reasonable representation of the cluster dynamics of SA-DMA nucleation
76 in three-dimensional (3-D) models is important for 3-D NPF modeling and subsequent
77 assessment of its impacts on environment and climate.

78 Empirical models in form of power law functions have been extensively utilized to
79 examine how particle formation rates respond to precursor concentrations (Semeniuk
80 and Dastoor, 2018). Through parameter fitting, these empirical models can effectively
81 reproduce the particle formation rates observed in both laboratory experiments and field
82 measurements (Kulmala et al., 2006; Riccobono et al., 2014; Semeniuk and Dastoor,
83 2018). Subsequently, they can be integrated into 3-D models for regional or global NPF
84 simulations. Bergman et al. (2015) and Dunne et al. (2016) have simulated SA-DMA
85 nucleation utilizing global models, which incorporate empirical equations derived from
86 experimental data obtained from CLOUD chamber or flow tube experiments. These
87 parameterization schemes successfully characterize the response of particle formation
88 rates to precursor concentrations, however, they fail to account for dependencies on T
89 and CS due to the ignorance of explicit cluster dynamics. As a result, they are identified
90 to be inadequate for accurately reproducing NPF events in winter Beijing (Li et al.,
91 2023).

92 We recently developed an analytical equation for SA-DMA nucleation
93 parameterization based on detailed cluster dynamics simulations (abbreviated as
94 `Dynamic_Sim`) (Li et al., 2023c). To derive an explicit equation, several simplifications
95 have been made in `Dynamic_Sim`, including 1) only $(SA)_k(DMA)_k$ ($k = 1-4$) and
96 $(SA)_2(DMA)_1$ clusters are considered; 2) clusters larger than $(SA)_1(DMA)_1$ are
97 regarded stable with no evaporation; and 3) $(SA)_4(DMA)_4$ cluster is the only terminal
98 cluster in calculating particle formation rates. Subsequent applications in 3-D modeling
99 have demonstrated significantly improved performance of `Dynamic_Sim` compared to
100 previous data-fitting parameterizations in simulating the particle formation rates, the
101 evolution of particle number size distributions (PNSDs), and NPF events in winter



102 Beijing. However, the efficacy of Dynamic_Sim in NPF simulation has yet to be
103 assessed under varying atmospheric conditions, such as the summer season
104 characterized by relatively higher T and lower CS compared to winter. Moreover, the
105 impacts of simplifications made in the derivation of Dynamic_Sim on 3-D NPF
106 simulation under different atmospheric conditions remain unclear.

107 Atmospheric Cluster Dynamics Code (ACDC) is a flexible box model for
108 simulating cluster dynamics and particle formation rates (Mcgrath et al., 2012). In
109 addition to representing T - and CS- dependencies for particle formation rate as
110 Dynamic_Sim, ACDC considers the source/sink terms of all given molecules/clusters
111 within a nucleation system without simplifications of the clustering processes. By
112 integrating quantum chemical calculations with ACDC, Almeida et al. (2013)
113 discovered that the simulated SA-DMA nucleation provides valuable insights for
114 interpreting the measurements from the CLOUD chamber experiments. Similarly, Lu
115 et al. (2020) demonstrated that ACDC coupled with quantum chemistry calculations
116 can effectively reproduce the particle formation rates observed in urban Shanghai.
117 While ACDC has been extensively utilized in box modeling (Almeida et al., 2013; Lu
118 et al., 2020; Yang et al., 2021), its potential for deriving parameterizations for 3-D
119 models has not been explored in previous studies. Furthermore, ACDC program in
120 modeling the nucleation process is highly reliant on specific thermodynamic data for
121 the molecular clusters of interest, which are primarily obtained through quantum
122 chemical calculations (Elm et al., 2020). The uncertainty surrounding the influence of
123 different quantum chemical calculation approaches adds additional complexity to the
124 application of ACDC-derived parameterization in 3-D NPF modeling.

125 This study aims to compare different cluster dynamic-based parameterizations for
126 SA-DMA nucleation and identify the robust one applicable for 3-D models. We
127 introduced new parameterizations developed using the ACDC program, incorporating
128 various quantum chemical calculations. Different cluster dynamic-based
129 parameterizations, including ACDC-derived ones as well as Dynamic_Sim, are
130 comprehensively compared and evaluated through a combination of box-model
131 simulations, 3-D modeling, and in-situ observational data. Our findings reveal that by
132 incorporating the latest theoretical understanding and complete representation of cluster
133 dynamics, ACDC-derived parameterization demonstrates reliable performance in 3-D
134 NPF simulation for both winter and summer conditions in Beijing and exhibits potential
135 applicability in diverse atmospheric conditions. The study sheds light on the impacts of
136 employing various simplifications in cluster dynamics and different theoretical
137 approaches in deriving parameterizations on NPF simulation. In addition to
138 contributing to the precise simulation of SA-DMA nucleation and the quantification of
139 its environmental and climatic effects, this study provides valuable references for
140 simulating other nucleation mechanisms in 3-D models.

141 **2 METHODS**

142 **2.1 Configurations of ACDC**

143 Here, $(SA)_m(DMA)_n$ clusters ($0 < n \leq m \leq 3$, n and m represent the number of SA



144 and DMA molecules in a cluster) are used to build the ACDC-derived parameterizations
145 for SA-DMA nucleation due to their reported much higher stability compared to those
146 containing more DMA molecules than SA molecules (Xie et al., 2017). The
147 conformations and thermodynamics of SA-DMA clusters are taken from our other
148 study (Ning et al., 2024). Briefly, the conformations of selected clusters are taken from
149 the reported global minima from Li et al. (2020), and the key thermodynamic data for
150 ACDC, Gibbs free energy change (ΔG), are recalculated at the DLPNO-CCSD(T)/aug-
151 cc-pVTZ// ω B97X-D/6-311++G(3df,3pd) level of theory. Based on benchmark studies
152 (Elm et al., 2020), this level of theory provides dependable thermodynamic insights into
153 molecular clusters during nucleation and represents the latest theoretical approach. In
154 addition, the rotational symmetry is consistently considered in quantum calculations
155 following Besel et al. (2020). Following most previous ACDC simulation studies (Xie
156 et al., 2017; Elm et al., 2020; Ning et al., 2020), $(SA)_4(DMA)_3$ and $(SA)_4(DMA)_4$
157 clusters are defined as the boundary conditions, i.e. the clusters fluxing out the
158 simulated system and participating in subsequent growth in ACDC simulations,
159 considering their high stability. Since clusters containing SA tetramers are estimated to
160 have an electrical mobility diameter of 1.4 nm (Cai et al., 2023; Jen et al., 2014; Thomas
161 et al., 2016), the formation rates of $(SA)_4(DMA)_3$ and $(SA)_4(DMA)_4$ clusters are
162 therefore deemed as the particle formation rates at 1.4 nm ($J_{1.4}$). Size-dependent
163 coagulation sink (CoagS) is counted for each SA-DMA cluster which is consistent with
164 Dynamic_Sim (Li et al., 2023c):

$$165 \quad \text{CoagS}_i = \text{CS} \left(\frac{V_i}{V_1} \right)^{1.7}$$

166 where V_i and V_1 (m^3) represent the volume of cluster i and SA molecule, respectively.
167 The power-law exponent of -1.7 is selected according to typical range in the atmosphere
168 (Lehtinen et al., 2007). In addition, enhancement for collision processes from Van de
169 Waals forces is also considered. We refer to the ACDC-derived parameterization in
170 coupling the DLPNO-CCSD(T)/aug-cc-pVTZ// ω B97X-D/6-311++G(3df,3pd) level of
171 theory and adequate cluster dynamics as ACDC_DB, which is established as the base-
172 case for our discussion of other cluster dynamics-based parameterizations.

173 In addition to the direct comparison of ACDC_DB to Dynamic_Sim, additional test
174 parameterizations combining ACDC_DB and three simplifications within
175 Dynamic_Sim are established and compared with ACDC_DB to further probe the
176 impacts of these simplifications on NPF simulations. The configurations of all
177 parameterizations are detailed in Table 1. It should be noted that when all
178 simplifications are applied on ACDC_DB, Dynamic_Sim still predicts higher $J_{1.4}$
179 compared to ACDC_DB (Figure S1A). This is because the ΔG value of the initial
180 $(SA)_1(DMA)_1$ cluster at 298.15 K used in Dynamic_Sim, which is taken from Myllys
181 et al. (Myllys et al., 2019), is slightly lower than that used in ACDC_DB (-13.5 kcal
182 mol^{-1} for Dynamic_Sim and -12.9 kcal mol^{-1} for ACDC_DB) (Ning et al., 2024), even
183 though both parameterizations employ the quantum chemical calculation method of
184 DLPNO-CCSD(T). Possible reasons for the discrepancy include the utilization of a



185 larger basis set (3-zeta 6-311++G(3df,3pd)) and higher convergence criteria (Tight
 186 PNO + Tight SCF) in this study compared to that in Myllys et al.. Aligning the ΔG for
 187 (SA)₁(DMA)₁ cluster in Dynamic_Sim with that of ACDC leads to a high consistency
 188 in the predicted $J_{1,4}$ between the two approaches (Figure S1B). The uncertainty of ΔG
 189 used in Dynamic_Sim is discussed in our previous study (Li et al., 2023c) and here we
 190 mainly focus on the impacts of simplifications in Dynamic_Sim.

191 While the DLPNO-CCSD(T)/aug-cc-pVTZ// ω B97X-D/6-311++G(3df,3pd) level
 192 of theory yields reasonable cluster thermodynamics, quantum chemistry calculations
 193 employing the RI-CC2 method predicting lower ΔG for cluster formation (stronger
 194 binding between molecules within clusters), has been widely used in conjunction with
 195 ACDC to interpret experimental and observed particle formation rates in previous
 196 studies (Almeida et al., 2013; Kürten et al., 2018; Ning et al., 2020). The prevalent
 197 combination used with the RI-CC2 method is RI-CC2/aug-cc-pV(T+d)Z//M06-2X/6-
 198 311++G(3df,3pd) level of theory (Lu et al., 2020; Liu et al., 2021; Ning et al., 2022;
 199 Ning and Zhang, 2022; Liu et al., 2019). Based on Elm's work, compared to DLPNO-
 200 CCSD(T)/aug-cc-pVTZ// ω B97X-D/6-311++G(3df,3pd), the differences in predicted
 201 cluster binding energies primarily stem from discrepancies between DLPNO-CCSD(T)
 202 and RI-CC2 in single-point energy calculations, while the ω B97X-D and M06-2X
 203 functionals exhibit similar performance (Elm et al., 2013; Elm et al., 2020). Also, in
 204 previous studies the RI-CC2 method combined with ACDC was consistently
 205 accompanied by application of a sticking factor (SF) of 0.5 in treating collision
 206 processes (Almeida et al., 2013; Lu et al., 2020). However, it is noteworthy that,
 207 according to Stolzenburg et al.'s work (Stolzenburg et al., 2020), the SF of the neutral
 208 SA-DMA cluster system should be unity. Here, we refer to the traditional theoretical
 209 approach as employing the RI-CC2/aug-cc-pV(T+d)Z//M06-2X/6-311++G(3df,3pd)
 210 level of theory and incorporating the SF of 0.5 in collision processes. An ACDC-derived
 211 parameterization coupling the traditional theoretical approach is established to assess
 212 the effectiveness of the traditional method in NPF simulation (ACDC_RM_SF0.5).
 213 Except for the varied thermodynamic inputs and SF, the remaining configurations of
 214 ACDC_RM_SF0.5 are identical to ACDC_DB. Additionally, we establish a test
 215 parameterization coupling RI-CC2/aug-cc-pV(T+d)Z//M06-2X/6-311++G(3df,3pd)
 216 level of theory with an SF of unity (ACDC_RM) to evaluate the impact solely arising
 217 from the quantum chemical calculation method. Note that SF of unity is applied to all
 218 parameterizations in this study except for the ACDC_RM_SF0.5.

219 To quantify the differences in simulating $J_{1,4}$ among different cluster dynamics-
 220 based parameterizations compared to our base-case ACDC_DB, we introduce a
 221 parameter R :

$$222 \quad R_X = \frac{\sum_i^n (X_i / \text{ACDC_DB}_i)}{n}$$

223 where ACDC_DB_{*i*} and X_{*i*} denote the simulated $J_{1,4}$ by the base-case ACDC_DB and
 224 another specific parameterization X, respectively, given the input scenarios of *i* (a set
 225 of input values for *T*, CS, concentration of SA ([SA]) and DMA ([DMA])), and *n*



226 signifies the total number of input scenarios.

227

228 **Table 1.** Summary of various cluster dynamics-based parameterizations of SA-DMA
 229 nucleation in this study (main parameterizations are in bold, while test ones in regular)

| Case | Description |
|----------------------|---|
| Dynamic_Sim | Reported parameterization from Li et al. 2023 combining the simplifications in boundary conditions, cluster evaporations, and cluster number |
| ACDC_DB | ACDC-derived parameterization coupling DLPNO-CCSD(T)/aug-cc-pVTZ// ω B97X-D/6-311++G(3df,3pd) level of theory, namely the latest theoretical approach |
| ACDC_DB_BC | ACDC-derived parameterization coupling DLPNO-CCSD(T)/aug-cc-pVTZ// ω B97X-D/6-311++G(3df,3pd) level of theory and simplification in boundary conditions (only $(SA)_4(DMA)_4$ cluster is set as boundary condition) |
| ACDC_DB_CE | ACDC-derived parameterization coupling DLPNO-CCSD(T)/aug-cc-pVTZ// ω B97X-D/6-311++G(3df,3pd) level of theory and simplification in cluster evaporations (the evaporation rates of $(SA)_k(DMA)_k$ ($k = 2-3$) and $(SA)_2(DMA)_1$ clusters are kept zero) |
| ACDC_DB_CN | ACDC-derived parameterization coupling DLPNO-CCSD(T)/aug-cc-pVTZ// ω B97X-D/6-311++G(3df,3pd) level of theory and simplification in cluster number (only $(SA)_k(DMA)_k$ ($k = 1-3$) and $(SA)_2(DMA)_1$ clusters are involved) |
| ACDC_RM_SF0.5 | ACDC-derived parameterization coupling RI-CC2/aug-cc-pV(T+d)Z//M06-2X/6-311++G(3df,3pd) level of theory and a SF of 0.5 is applied in collision process, namely the traditional theoretical approach |
| ACDC_RM | ACDC-derived parameterization coupling RI-CC2/aug-cc-pV(T+d)Z//M06-2X/6-311++G(3df,3pd) level of theory and a SF of 1 is applied |

230

231 **2.2 Incorporating the ACDC-derived Parameterizations into WRF-Chem/R2D-**
 232 **VBS Model**

233 Various parameterizations are subsequently implemented in the Weather Research
 234 and Forecasting-Chemistry model (WRF-Chem) integrating an experimentally
 235 constrained Radical Two-Dimensional Volatility Basis Set (2D-VBS) (denoted as
 236 WRF-Chem/R2D-VBS) (Zhao et al., 2020). Incorporating the box-model ACDC into a
 237 3-D model using the explicit mathematical formula, as Dynamic_Sim, proves to be
 238 challenging. Here, we created a four-dimensional look-up table that delineates the



239 response of $J_{1.4}$ to four input variables (T , CS, [SA], and [DMA]) for each ACDC-
240 derived parameterization (Yu, 2010). The table is derived based on multiple ACDC runs
241 by varying input variables. The ranges for the input variables correspond to typical
242 conditions of the atmosphere. Except for T , the ranges of variation for all other variables
243 exceed at least one order of magnitude. Therefore, temperature is assumed to follow
244 arithmetic uniform distribution, while the other variables are assumed to follow
245 geometric uniform distribution. Details for the input variables are given in Table S1. In
246 WRF-Chem/R2D-VBS simulations, $J_{1.4}$ are online calculated by interpolating values
247 from a look-up table based on real-time input parameters. In our previous study, we
248 have developed an emission inventory for China and its surrounding regions (Li et al.,
249 2023c). Here [DMA] is calculated in WRF-Chem/R2D-VBS based on a comprehensive
250 source-sink representation of DMA. More details of including DMA in WRF-
251 Chem/R2D-VBS can be found in our previous study (Li et al., 2023c). In addition, a
252 time-integrated-average [DMA] as well as [SA] of each time step were used to drive
253 SA-DMA nucleation, since SA-DMA nucleation is accompanied with condensation of
254 gaseous SA and DMA on pre-existing aerosols simultaneously in the atmosphere.

255 Besides SA-DMA nucleation, seven other nucleation mechanisms have already
256 been incorporated in WRF-Chem/R2D-VBS (Zhao et al., 2020), including neutral/ion-
257 induced $\text{H}_2\text{SO}_4\text{-H}_2\text{O}$ nucleation, neutral/ion-induced $\text{H}_2\text{SO}_4\text{-NH}_3\text{-H}_2\text{O}$ nucleation,
258 neutral/ion-induced pure organics nucleation, and $\text{H}_2\text{SO}_4\text{-organics}$ nucleation. The
259 organics involved in nucleation are ultralow- and extremely low-volatility organic
260 compounds (ULVOC and ELVOC) with $\text{O:C} > 0.4$. The formation chemistry of ULVOC
261 and ELVOC from monoterpenes, including autoxidation and dimerization, is traced by
262 the R2D-VBS framework (Zhao et al., 2020). Note that the impact of the other seven
263 mechanisms on particle formation rates and particle number concentration is low
264 compared to SA-DMA as revealed by our previous study (Li et al., 2023c). In WRF-
265 Chem/R2D-VBS, the evolution of PNSDs from 1 nm to 10 μm is treated by MOSAIC
266 (Model for Simulating Aerosol Interactions and Chemistry) module. The newly formed
267 1.4 nm particles from SA-DMA nucleation are injected into the smallest size bin (1 -
268 1.5 nm) of the MOSAIC.

269 **2.3 Configurations of WRF-Chem/R2D-VBS Model**

270 The WRF-Chem/R2D-VBS model, incorporating various cluster dynamics-based
271 SA-DMA nucleation parameterizations, was employed in a simulation over a domain
272 with a spatial resolution of 27 km. This domain covers eastern Asia, with Beijing
273 situated close to the center of the simulation area. Details of model configurations can
274 be found in our previous study (Li et al., 2023c). Briefly, we use the ABaCAS-EI 2017
275 and IIASA 2015 emission inventories for mainland China and other areas in the domain,
276 respectively, to represent the anthropogenic emissions (Zheng et al., 2019; Li et al.,
277 2017; Li et al., 2023b); we use Model of Emissions of Gases and Aerosols from Nature
278 (MEGAN) v2.04 to calculate the biogenic emissions (Guenther et al., 2006). The
279 simulation results from the National Center for Atmospheric Research's Community
280 Atmosphere Model with Chemistry ([9](https://www.acom.ucar.edu/cam-chem/cam-</p></div><div data-bbox=)



281 chem.shtml) is used for the chemical initial and boundary conditions in WRF-
282 Chem/R2D-VBS simulations.

283 The simulation period consists of two parts: the winter period, which spans from
284 January 14 to January 31, 2019, and the summer period, which is from August 18 to
285 August 31, 2019. Previous observational studies have shown that the particle formation
286 rates reach their highest and lowest levels during winter and summer in China,
287 respectively (Deng et al., 2020; Chu et al., 2019). Therefore, periods from these two
288 seasons are selected as representative simulation periods in this study and the specific
289 time periods corresponded to those with relatively complete and continuous PNSDs and
290 $J_{1.4}$ observations. Since observational data for DMA concentration is only available for
291 the period from January 1, 2019 to January 23, 2019, similar to our other study (Ning
292 et al., 2024), we performed additional simulation for this period to compare
293 observational and simulated DMA concentrations. For each season, all the SA-DMA
294 parameterizations listed in Table 1 were employed for simulation. Among them,
295 ACDC_DB, Dynamic_Sim, and ACDC_RM_SF0.5 serve as three main
296 parameterizations, while ACDC_DB_CE, ACDC_DB_BC, ACDC_DB_CN, and
297 ACDC_RM are set as test cases to investigate the impact of individual simplification
298 or theoretical approach on NPF simulations. In all comparisons, ACDC_DB is set as a
299 reference.

300 **2.4 Ambient Measurements**

301 In the 3-D simulations, we utilize measured concentrations of nucleation precursors
302 and PNSDs as a criterion to discuss the model performance with various
303 parameterizations. The duration of the observational data matches that of the
304 simulations mentioned above. Detailed descriptions of the observation site and
305 instruments can be found in our previous research (Deng et al., 2020). Briefly, the
306 observation site is located on the West Campus of the Beijing University of Chemical
307 Technology. CI-TOF-MS (chemical ionization time-of-flight mass spectrometer;
308 Aerodyne Research Inc.) were used to measure the concentrations of SA. Amine
309 concentrations were measured with a modified TOF-MS using H_3O^+ or its clusters as
310 the reagent ions. PNSDs from 1 nm to 10 μm were measured using a PSD (particle size
311 distribution) system and a DEG-SMPS (diethyl glycol scanning mobility particle
312 spectrometer). $J_{1.4}$ derived from observation is calculated employing an improved
313 aerosol population balance formula (Cai and Jiang, 2017).

314

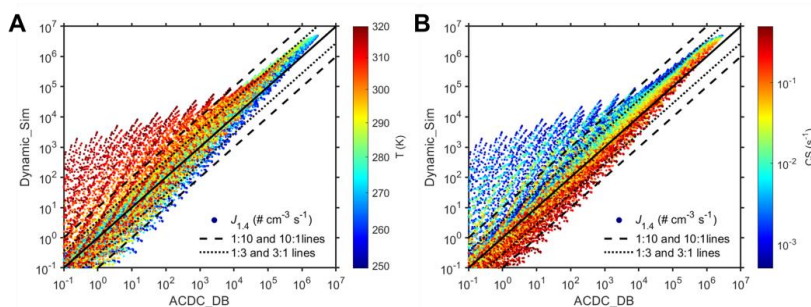


315 **3 RESULTS AND DISCUSSIONS**

316 **3.1 Comparison of Different Parameterizations Based on Box-Model Simulations**

317 **3.1.1 Comparison between ACDC_DB and Dynamic_Sim**

318 **Figure 1** illustrates the comparison between the reported cluster dynamics-based
 319 parameterization with simplifications, Dynamic_Sim, and the base-case
 320 parameterization ACDC_DB. The comparison is based on a comprehensive dataset that
 321 includes over 40,000 box-model simulations for each parameterization, by varying
 322 parameters such as [SA] ($1 \times 10^5 - 1 \times 10^8$ molec. cm^{-3}), [DMA] ($5 \times 10^6 - 1 \times 10^8$
 323 molec. cm^{-3}), CS ($5 \times 10^{-4} - 5 \times 10^{-1}$ s^{-1}), and T (250 – 320 K). In most scenarios, $J_{1,4}$
 324 predicted by ACDC_DB and Dynamic_Sim demonstrates deviations within one order
 325 of magnitude, with the majority falling within a factor of 3. However, Dynamic_Sim
 326 predicts notably higher $J_{1,4}$ than ACDC_DB in scenarios where T exceeds ~ 300 K and
 327 CS is below $\sim 3 \times 10^{-3}$ s^{-1} , characteristic of a clean atmosphere during summer. The
 328 discrepancy in these scenarios elevates the overall $R_{\text{Dynamic_Sim}}$ up to 17.0. Furthermore,
 329 no clear correlation is observed between the differences of the two parameterizations
 330 and other input parameters such as [DMA] and [SA] (**Figure S2**). The differences
 331 between parameterizations are attributed to the combined effects of the three
 332 simplifications and the lower ΔG of (SA)₁(DMA)₁ cluster in Dynamic_Sim. However,
 333 the latter should not be the primary cause for the significant differences of $J_{1,4}$ prediction
 334 under high T and low CS conditions, as it typically results in an overestimation within
 335 an order of magnitude ($R=3.3$) (**Figure S1**).
 336



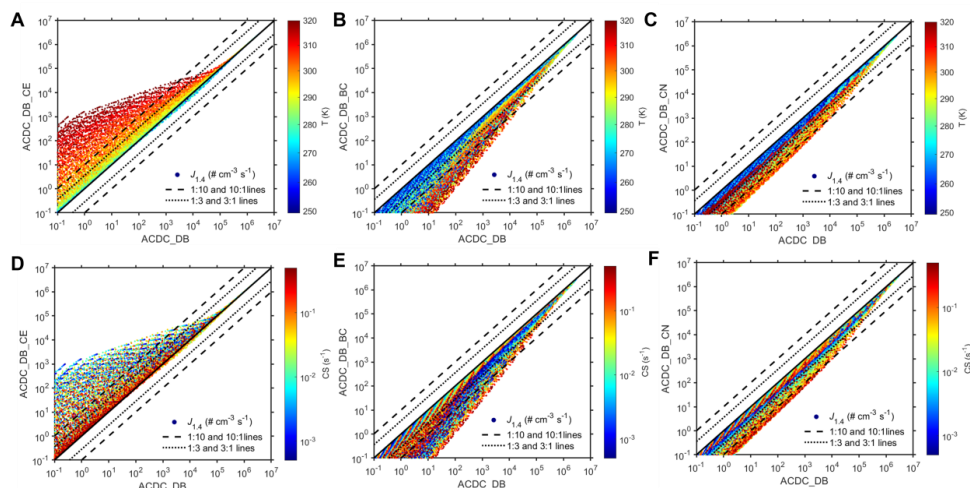
337 **Figure 1.** Comparison of $J_{1,4}$ predictions between ACDC_DB and Dynamic_Sim
 338 correlated with T variation (A) and CS variation (B). Solid dots represent simulated $J_{1,4}$
 339 values, solid lines indicate a 1:1 line, dotted lines correspond to 1:3 and 3:1 lines, and
 340 dashed lines represent 1:10 and 10:1 lines.
 341

342
 343 The impacts of the three simplifications made in Dynamic_Sim are shown in **Figure**
 344 **2**. Specifically, the simplification in cluster evaporations tends to elevate the predicted
 345 $J_{1,4}$, whereas the simplifications in boundary conditions and cluster number tend to
 346 lower them. When applying the simplification in cluster evaporations (clusters larger
 347 than (SA)₁(DMA)₁ are regarded stable with no evaporation) to ACDC_DB, the
 348 predicted $J_{1,4}$ by ACDC_DB_CE only slightly exceed than that of ACDC_DB within a



349 factor of 3 under conditions where $T < \sim 290$ K and $CS > \sim 0.1$ s⁻¹. However, the
 350 overestimation of $J_{1,4}$ prediction by ACDC_DB_CE becomes much greater with
 351 increasing T and decreasing CS . The discrepancy between ACDC_DB_CE and
 352 ACDC_DB should be primarily attributed to the pivotal role of T in influencing cluster
 353 evaporation rates (Ortega et al., 2012; Deng et al., 2020). At low T , the evaporation
 354 rates of clusters are low enough to allow efficient nucleation, thus whether setting the
 355 concerned SA-DMA clusters to evaporate based on the expected evaporation rates does
 356 not lead to a significant impact on $J_{1,4}$ prediction. However, at high T , the evaporation
 357 rates of clusters significantly increase, therefore the simplification in cluster
 358 evaporations within ACDC_DB_CE is likely to predict higher $J_{1,4}$ than those with no
 359 simplification. The impact of simplification in cluster evaporations across varying T is
 360 also found in a nonbranched SA-DMA nucleation scheme from 280 K to 298 K reported
 361 by Li et al. (2023a). Note also that the overestimation of ACDC_DB_CE diminishes as
 362 CS increases (Figure 2D), with CS becoming the primary sink in the nucleation system
 363 and the impact of cluster evaporations becoming less pronounced. This underscores the
 364 connection between the specific deviation arising from simplification in cluster
 365 evaporations and the respective contributions of CS and cluster evaporations to the
 366 overall sink for clusters in nucleation. In addition, the relative independence of the
 367 differences between ACDC_DB_CE and ACDC_DB from variations in precursor
 368 concentrations ($[SA]$ and $[DMA]$) is similar to that between Dynamic_Sim and
 369 ACDC_DB (Figure S3). Overall, the scenarios where ACDC_DB_CE predicts higher
 370 $J_{1,4}$ than ACDC_DB only occurs under conditions of both high T and low CS (Figure
 371 2A and Figure 2D). The averaged discrepancy between ACDC_DB_CE and
 372 ACDC_DB $R_{ACDC_DB_CE}$ is 22.3, closely resembling $R_{Dynamic_Sim}$, indicating that the
 373 simplification in cluster evaporations is a major factor contributing to the difference
 374 between Dynamic_Sim and ACDC_DB.

375



376

377

Figure 2. Comparison of $J_{1,4}$ predictions between ACDC_DB and test cases including



378 ACDC_DB_CE (A and D), ACDC_DB_BC (B and E), and ACDC_DB_CN (C and F).
379 The first row in the panel (A, B and C) is correlated with T variation and the second
380 row (D, E and F) is correlated with CS variation. Solid dots represent simulated $J_{1,4}$
381 values, solid lines indicate a 1:1 line, dotted lines correspond to 1:3 and 3:1 lines, and
382 dashed lines represent 1:10 and 10:1 lines.

383

384 The underestimations of ACDC_DB_BC and ACDC_DB_CN in $J_{1,4}$ prediction
385 compared to base-case ACDC_DB are related to the growth pathways of SA-DMA
386 clusters. In the original scheme of ACDC_DB, precursor molecules have the flexibility
387 to pass through any $(SA)_m(DMA)_n$ clusters ($0 < n \leq m \leq 3$), and terminal 1.4-nm
388 particles are formed when the clusters grow to $(SA)_4(DMA)_4$ or $(SA)_4(DMA)_3$. As
389 expected, ACDC_DB_BC, which assumes $(SA)_4(DMA)_4$ cluster as the only boundary
390 condition with an omission of $(SA)_4(DMA)_3$ cluster, predicts lower $J_{1,4}$ than ACDC_DB.
391 $(SA)_4(DMA)_3$ and $(SA)_4(DMA)_4$ clusters are primarily formed from $(SA)_3(DMA)_3$
392 cluster by colliding with a SA molecule and a $(SA)_1(DMA)_1$ cluster, respectively. As
393 the concentration of $(SA)_1(DMA)_1$ cluster is more sensitive to T , we further found that
394 the discrepancy between ACDC_DB_BC and ACDC_DB becomes more pronounced
395 with increasing T (Figure 2B). Furthermore, we found no apparent correlation between
396 the variation of CS and the disparity between ACDC_DB_BC and ACDC_DB (Figure
397 2E).

398 In addition to ACDC_DB_BC, ACDC_DB_CN also underestimates $J_{1,4}$ compared
399 to ACDC_DB with a comparable value (~ 0.5) of $R_{ACDC_DB_CN}$ and $R_{ACDC_DB_BC}$. Under
400 the simplification in cluster number, the formation of 1.4-nm clusters can only occur
401 through specific pathways, including $(SA)_1(DMA)_1 \rightarrow (SA)_2(DMA)_2 \rightarrow (SA)_3(DMA)_3$
402 $\rightarrow (SA)_4(DMA)_4/(SA)_4(DMA)_3$, $(SA)_1(DMA)_1 \rightarrow (SA)_2(DMA)_1 \rightarrow (SA)_2(DMA)_2 \rightarrow$
403 $(SA)_3(DMA)_3 \rightarrow (SA)_4(DMA)_4/(SA)_4(DMA)_3$, or a combination thereof, while other
404 pathways are restricted. Due to the variability in growth pathways and their
405 contributions to $J_{1,4}$ under different atmospheric conditions, the difference between
406 ACDC_DB_CN and ACDC_DB is not strongly correlated with the variations of T and
407 CS (Figure 2C and Figure 2F). Despite that, while the differences between the two
408 tested parameterizations (ACDC_DB_BC and ACDC_DB_CN) involving cluster
409 growth pathways and the original ACDC_DB are not highly correlated with [DMA],
410 there is a more pronounced correlation with [SA], which implies a more important role
411 of SA in cluster growth (Figure S4 and Figure S5).

412 In our previous study, we demonstrated improvements in computing CS-dependent
413 $J_{1,4}$ of SA-DMA nucleation with the Dynamic_Sim compared to the previous power-
414 law parameterizations under polluted atmospheric conditions (Li et al., 2023c). Here,
415 we further show that, based on Dynamic_Sim, the new ACDC_DB with complete
416 cluster dynamics can more reasonably simulate $J_{1,4}$ under previously less studied
417 conditions of high T ($> \sim 300$ K) and low CS ($< \sim 3 \times 10^{-3} \text{ s}^{-1}$), where Dynamic_Sim tends
418 to produce significant overestimation of $J_{1,4}$. This overestimation is primarily driven by
419 the simplification in cluster evaporations within Dynamic_Sim. Even though a

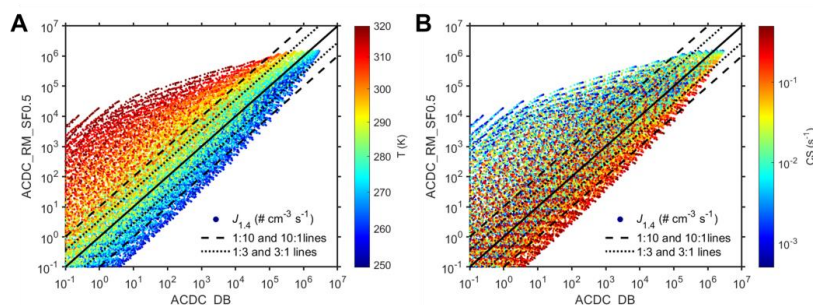


420 comparable performance in $J_{1,4}$ prediction between ACDC_DB and Dynamic_Sim
 421 could be achieved under other ambient conditions, cautions should be made that the
 422 mutual offsetting effect between overestimation and underestimation resulting from
 423 different simplifications in Dynamic_Sim when computing $J_{1,4}$.

424 3.1.2 Comparison between ACDC_DB and ACDC_RM_SF0.5

425 In Figure 3, ACDC_DB is compared with another main ACDC-derived
 426 parameterization, ACDC_RM_SF0.5, which uses the RI-CC2/aug-cc-pV(T+d)Z//M06-
 427 2X/6-311++G(3df,3pd) level of theory and employs a SF of 0.5 in processing collision.
 428 It can be observed that at lower temperatures (~ 280 K), ACDC_RM_SF0.5 and
 429 ACDC_DB exhibit similar performance in predicting $J_{1,4}$. However, with higher T
 430 (accompanied by lower CS with a slight dependency), $J_{1,4}$ predicted by
 431 ACDC_RM_SF0.5 become higher than that predicted by ACDC_DB, reaching even
 432 several orders of magnitude at the upper limit of the T range (320 K). Furthermore, we
 433 also observed that in scenarios close to the lower limit of the T range (250 K), the $J_{1,4}$
 434 predicted by ACDC_RM_SF0.5 shift from being higher to lower compared to
 435 ACDC_DB.

436



437

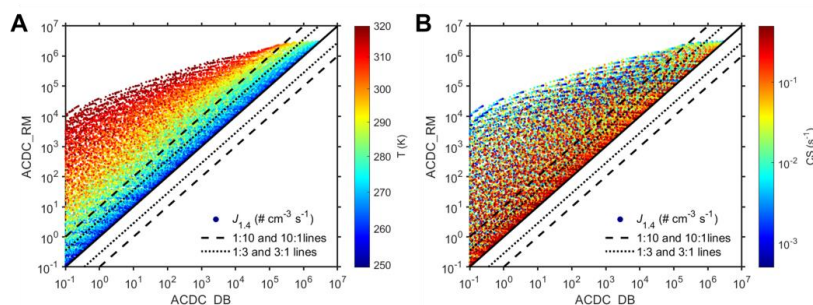
438 **Figure 3.** Comparison of $J_{1,4}$ predictions between ACDC_DB and ACDC_RM_SF0.5
 439 correlated with T variation (A) and CS variation (B). Solid dots represent simulated $J_{1,4}$
 440 values, solid lines indicate a 1:1 line, dotted lines correspond to 1:3 and 3:1 lines,
 441 and dashed lines represent 1:10 and 10:1 lines.

442

443 The distinction between ACDC_RM_SF0.5 and ACDC_DB arises from the
 444 combined effects of variation in quantum chemical calculation method and the
 445 application of the 0.5 SF in collision processing. As depicted in Figure 4, when the SF
 446 in ACDC_RM_SF0.5 is set to unity as in ACDC_DB, the resulting ACDC_RM
 447 parameterization predicts consistently higher $J_{1,4}$ than ACDC_DB. This implies that the
 448 modified quantum chemical calculation method, which results in lower evaporation
 449 rates for clusters within the system compared to ACDC_DB under the same condition,
 450 leads to higher $J_{1,4}$ predictions. The impact from varying quantum chemical calculation
 451 method is akin to that from simplification in cluster evaporations discussed earlier. The
 452 distinction between ACDC_RM and ACDC_DB_CE lies in the fact that the modified
 453 quantum chemical calculation method affects all clusters within the system, whereas



454 the simplification in cluster evaporations is specific to limited clusters. This contributes
 455 to a much higher R_{ACDC_RM} (614.5) compared to $R_{ACDC_DB_CE}$ (22.3). Despite that,
 456 compared to ACDC_DB, the differences for both ACDC_DB_CE, ACDC_RM, as well
 457 as ACDC_RM_SF0.5 demonstrate similar sensitivity to T (Figure 3A and Figure 4A)
 458 and CS (Figure 3B and Figure 4B) but independence on [SA] (Figure S6A and Figure
 459 S7A) and [DMA] (Figure S6B and Figure S7B). Comparing ACDC_RM_SF0.5 and
 460 ACDC_RM, it can be inferred that the application of a 0.5 SF in collision processes
 461 would result in an underestimation in $J_{1.4}$ prediction. It can be noted that in most
 462 previous studies (Almeida et al., 2013; Kürten et al., 2018; Elm et al., 2020),
 463 comparisons of ACDC simulations using the traditional method and measured particle
 464 formation rates are conducted at around 280 K. At this temperature, all three main
 465 parameterizations of ACDC_RM, ACDC_DB, and Dynamic_Sim tends to yield similar
 466 $J_{1.4}$ predictions and should have consistent applicability in NPF simulation.
 467



468 **Figure 4.** Comparison of $J_{1.4}$ predictions between ACDC_DB and ACDC_RM
 469 correlated with T variation (A) and CS variation (B). Solid dots represent simulated $J_{1.4}$
 470 values, solid lines indicate a 1:1 line, dotted lines correspond to 1:3 and 3:1 lines, and
 471 dashed lines represent 1:10 and 10:1 lines.
 472

473
 474 In summary, based on our base-case parameterization ACDC_DB, the extensive
 475 box model simulations above demonstrate the characteristics and applicability
 476 conditions of different parameterizations. Specifically, Dynamic_Sim is applicable
 477 under most atmospheric conditions with $T < \sim 300$ K and $CS > \sim 3.0 \times 10^{-3} \text{ s}^{-1}$, while
 478 ACDC_RM_SF0.5 is suitable under conditions with T around 280 K. We further use
 479 reported measurements from well-controlled CLOUD chamber experiments to examine
 480 the characteristics and applicability of these parameterizations (Xiao et al., 2021). As
 481 shown in Figure S8, simulations using three main parameterizations, ACDC_DB,
 482 ACDC_RM, and Dynamic_Sim, correspond well to experimental results at low
 483 temperature ($T = 278$ K), proving the applicability of all three parameterizations at this
 484 temperature. In the experiments with elevated temperature ($T = 293$ K), ACDC_DB and
 485 Dynamic_Sim continues to exhibit similar performance, with simulated results still
 486 corresponding to experimental results. In contrast, ACDC_RM_SF0.5 only shows a
 487 slight T -dependence, which is deviated from the measurements. The comparison



488 between controlled experiments and box-model simulations hence confirms our
489 conclusions above, and provides a solid basis for further discussions on 3-D simulations
490 using these parameterizations with constraint from field observations.

491 **3.2 Comparison of Different Parameterizations Based on 3-D Model Simulations**

492 Various cluster dynamics-based parameterizations for SA-DMA nucleation were
493 subsequently integrated into the WRF-Chem/R2D-VBS model. 3-D simulations using
494 these parameterizations have been conducted for both wintertime and summertime
495 conditions in Beijing. Given that the concentrations of precursors are crucial input
496 variables for each parameterization, the simulated and observed concentrations of
497 [DMA] and [SA] are compared. Figure S9, Figure S10 and Table S2 illustrates good
498 consistencies in temporal variations and the mean values between simulations and
499 observations in Beijing. This validates the reliability of our representation of sources
500 and sinks for nucleating precursors and serves as a foundation for our discussions on
501 the performances of various parameterizations. In the following sections, we discuss
502 the results of 3-D NPF simulations in Beijing during winter and summer by employing
503 different parameterizations. The evaluation of various parameterizations focuses on
504 their ability to reproduce in situ NPF measurements across different seasons.

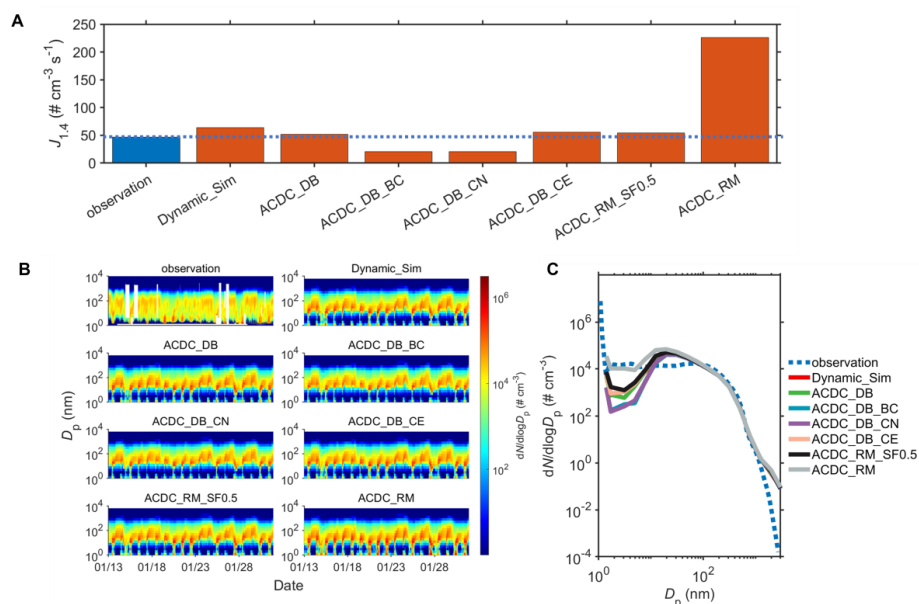
505 **3.2.1 Wintertime Simulations**

506 Figure 5A and Figure S11A primarily compare the simulated $J_{1.4}$ values from
507 different parameterizations with those derived from wintertime observations in Beijing,
508 as $J_{1.4}$ being a key parameter describing NPF events. The performance of Dynamic_Sim
509 in simulating $J_{1.4}$ during wintertime Beijing has been discussed in our previous study
510 (Li et al., 2023c). The averaged $J_{1.4}$ simulated by three main parameterizations
511 (Dynamic_Sim: $64.0 \text{ cm}^{-3} \text{ s}^{-1}$; ACDC_DB: $51.6 \text{ cm}^{-3} \text{ s}^{-1}$; ACDC_RM_SF0.5: 54.5 cm^{-3}
512 s^{-1}) approximate the observation ($46.7 \text{ cm}^{-3} \text{ s}^{-1}$). For test cases, however, only
513 ACDC_DB_CE ($55.7 \text{ cm}^{-3} \text{ s}^{-1}$) demonstrates a reasonable representation of $J_{1.4}$. $J_{1.4}$
514 simulated from ACDC_DB_BC ($20.5 \text{ cm}^{-3} \text{ s}^{-1}$) and ACDC_DB_CN ($20.8 \text{ cm}^{-3} \text{ s}^{-1}$) are
515 approximately two times lower than the observed values, while ACDC_RM (226.2 cm^{-3}
516 s^{-1}) is approximately five times higher than the observations.

517 The performances of different parameterizations on depicting $J_{1.4}$ subsequently
518 influences their representations of PNSDs evolution and NPF events, which are shown
519 in Figure 5B. Generally, most parameterizations efficiently reproduce the observed time
520 evolution of PNSDs and captures NPF events, such as those on 01/20, 01/21, 01/30,
521 and 01/31, which are characterized by the burst of aerosol number concentrations in
522 nanometer-sized range. Simulations using ACDC_DB_BC and ACDC_DB_CN result
523 in lower particle concentrations in the low size range (1-10 nm) during the NPF period
524 compared to three main parameterizations and the observations, while simulations with
525 ACDC_RM show higher concentrations, This is consistent with the comparison of $J_{1.4}$
526 among different parameterizations and further evident by the comparison of averaged
527 PNSDs in Figure 5C. Notably, when compared to observations, all parameterizations
528 consistently underestimate the averaged PNSDs within the 2-10 nm range but
529 overestimate them in the 10-50 nm range. This discrepancy may stem from simplified



530 assumptions in particle growth simulation, as discussed in our previous study (Li et al.,
 531 2023c).
 532
 533



534
 535 **Figure 5.** Comparison of simulated particle formation rates and particle number size
 536 distributions (PNSDs) with observations during January 13, 2019, to January 31, 2019,
 537 in Beijing. A represents the averaged particle formation rates during the period, the blue
 538 bars and orange bars represent observations and simulations, respectively, while the
 539 blue dashed line represents the observed values. Daily maximum values of $J_{1,4}$ are used
 540 following Deng et al. (2020); B for the time series of PNSDs; and C for the averaged
 541 PNSDs.

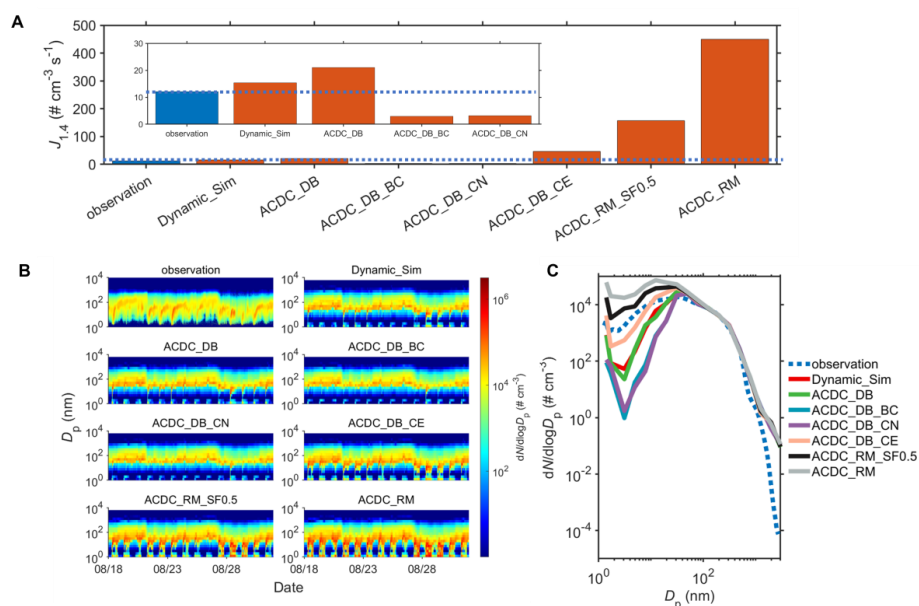
542
 543 The results show the applicability of all three main parameterizations in NPF
 544 modeling during wintertime periods. Importantly, the reliability of the new ACDC-
 545 derived parameterization based on the latest theoretical approach (ACDC_DB) without
 546 simplifications in 3-D NPF simulation, is affirmed. The differences among various
 547 parameterizations can be explained by the comprehensive box-model simulations
 548 above at corresponding conditions. Compared to ACDC_DB, the $J_{1,4}$ and PNSDs
 549 simulated by other two main parameterizations (Dynamic_Sim and ACDC_RM_SF0.5)
 550 agree similarly with observations, but for different reasons. In the case of Dynamic_Sim,
 551 the simplification in cluster evaporations has minimal impact on NPF simulation since
 552 CS is the dominant sink for clusters under the wintertime conditions (averaged T and
 553 CS is 274.7 K and $3.3 \times 10^{-2} \text{ s}^{-1}$, respectively). However, the simplifications in boundary
 554 conditions and cluster number lead to the underestimation of the $J_{1,4}$, consequently



555 lowering the simulated particle number concentrations in 1-100 nm size range due to
556 the ignorance of clusters contributing to growth. As a result, the agreement of
557 Dynamic_sim to observations should result from a combination of underestimation due
558 to simplifications in boundary conditions and cluster number, along with the
559 compensatory effect of the overestimation caused by lower ΔG for $(SA)_i(DMA)_i$
560 cluster. For another main parameterization ACDC_RM_SF0.5, since the test
561 parameterization ACDC_RM considerably overestimates $J_{1.4}$ and PNSDs compared to
562 the observations, the general agreement between ACDC_RM_SF0.5 and observations
563 should be attributed to a balance between reduced kinetic limit through the application
564 of SF and the compensatory effect of the overestimation caused by inappropriate
565 representation of cluster thermodynamics.

566 **3.2.2 Summertime Simulations**

567 Figure 6 provides additional insight into the performance of various
568 parameterizations in NPF simulation during summer. It can be noted that there exists a
569 significant difference in particle formation rates between winter and summer in Beijing.
570 As shown in Figure 6 and Figure S11B, ACDC_DB and Dynamic_Sim continues to
571 demonstrate consistent and effective performance in simulating $J_{1.4}$ (within a factor of
572 2), PNSDs evolution as well as NPF events. However, distinct differences emerge in
573 the NPF simulation for other parameterizations, including another main
574 parameterization ACDC_RM_SF0.5. Specifically, in contrast to the good performance
575 of ACDC_DB and Dynamic_Sim, ACDC_RM_SF0.5, along with the test case
576 ACDC_RM, exhibits a significant overestimation of $J_{1.4}$, exceeding the observations by
577 more than 15 times and over two orders of magnitude, respectively. This aligns with
578 their overestimation of NPF occurrences and particle number concentration in the size
579 range of 1-100 nm in comparison to observation, with a more pronounced
580 overestimation for ACDC_RM. Conversely, the test cases of ACDC_DB_BC and
581 ACDC_DB_CN show an underestimation of averaged $J_{1.4}$ by approximately 4-5 times.
582 They almost fail to depict NPF events, resulting in a significant underestimation of
583 number concentrations in the 1-100 nm size range. Simulations using ACDC_DB_CE
584 notably overestimates $J_{1.4}$ especially on 08/28 – 08/31 (Figure S11B), which results in
585 an overestimation of averaged $J_{1.4}$ by approximately 4 times compared to the
586 observations. However, apart from a moderate overestimation in the initial particle size,
587 we can observe a closer alignment of particle number concentrations in the 2-100 nm
588 range with observations for ACDC_DB_CE, which should result from a combination
589 of surplus newly formed particles and fast particle growth from inadequate assumptions
590 within the model.
591



592

593 **Figure 6.** Comparison of simulated particle formation rates and particle number size
 594 distributions (PNSDs) with observations during August 18, 2019, to August 31, 2019,
 595 in Beijing. A represents the averaged particle formation rates during the period, the blue
 596 bars and orange bars represent observations and simulations, respectively, while the
 597 blue dashed line represents the observed values. Daily maximum values of $J_{1,4}$ are used
 598 following Deng et al. (2020); B for the time series of PNSDs; and C for the averaged
 599 PNSDs.

600

601 Most previous NPF studies combining experiments/observations with simulations
 602 are conducted under conditions biased towards winter ($\sim 280\text{K}$) (Almeida et al., 2013;
 603 Lu et al., 2020). Under summer conditions with elevated T , there exists a deficiency in
 604 parameterization evaluations for simulating NPF. The 3-D simulation results during the
 605 summer period provide additional validation for the reliability of ACDC_DB. For
 606 ACDC_RM_SF0.5, evidence from both box-model simulations and 3-D simulations
 607 suggests that it can accurately reproduce real SA-DMA nucleation at temperatures
 608 around 280 K, while it has limitations in higher temperatures. Another main
 609 parameterization Dynamic_Sim consistently demonstrates good performance in NPF
 610 simulation, akin to its efficacy in winter conditions. With the increased temperature in
 611 summer (averaged T is 298.2 K), the influence of simplifications in cluster evaporations,
 612 cluster number, and boundary conditions becomes more profound, mirroring the trends
 613 observed in box-model simulations above. This leads to more significant
 614 overestimation for ACDC_DB_CE, and underestimation for ACDC_DB_CN and
 615 ACDC_DB_BC compared to the observation as well as the base-case ACDC_DB. Note
 616 that CS during the summer period (averaged CS is $2.8 \times 10^{-2} \text{ s}^{-1}$) decreases compared to



617 winter but remains significantly higher than typical values in clean regions ($\sim 3.0 \times 10^{-3}$
618 s^{-1}) (Dal Maso et al., 2008). According to the limited conditions for Dynamic_Sim
619 described above, although the overestimation of $J_{1,4}$ prediction resulting from the
620 simplification in cluster evaporations is more pronounced in summer compared to that
621 in winter, impacts from diverse overestimations and underestimations from different
622 simplifications and varied thermodynamics for $(SA)_1(DMA)_1$ cluster can still offset
623 each other, thereby allowing Dynamic_Sim to match observations. Based on previous
624 comparisons using box-models, significant differences in $J_{1,4}$ predictions between
625 Dynamic_Sim and ACDC_DB only exist under conditions of high $T > \sim 300$ K and low
626 $CS < \sim 3 \times 10^{-3} s^{-1}$, thus similar performance of Dynamic_Sim and ACDC_DB can be
627 expected in the polluted atmosphere ($CS > \sim 1.0 \times 10^{-2} s^{-1}$). In clean atmosphere with
628 high temperature, however, caution is advised when using Dynamic_Sim for 3-D NPF
629 simulations.

630 4. CONCLUSIONS

631 By integrating box modeling, 3-D simulations, also under the constraint from in
632 situ measurements, this study conducts comprehensive comparison of different cluster
633 dynamics-based parameterizations for SA-DMA nucleation. Among them, the ACDC-
634 derived parameterization grounded in the latest molecular-level understanding and
635 complete representation of cluster dynamics (ACDC_DB), is identified to effectively
636 model particle formation rates and PNSDs evolution in both winter and summer in
637 Beijing within 3-D simulations. While a previously proposed simplified cluster
638 dynamics-based parameterization (Dynamic_Sim) performs comparably in modeling
639 NPF in Beijing, analysis reveals that their similarity arises from a delicate balance
640 between overestimation and underestimation due to simplifications in cluster dynamics
641 processes and the difference in thermodynamics of initial cluster. Particularly, under
642 specific conditions of high temperature ($> \sim 300$ K) and low $CS (< \sim 3 \times 10^{-3} s^{-1})$,
643 Dynamic_Sim tends to make significant overestimation of particle formation rates
644 compared to the reality. Moreover, the study furnishes evidence that integrating ACDC-
645 derived parameterizations with the traditional theoretical approach RI-CC2/aug-cc-
646 pV(T+d)Z//M06-2X/6-311++G(3df,3pd) (ACDC_RM_SF0.5) effectively captures
647 particle formation rates and the evolution of PNSDs around 280 K, a temperature range
648 frequently explored in prior experiments and simulations investigating NPF (Kirkby et
649 al., 2011; Almeida et al., 2013; Kirkby et al., 2016; Xie et al., 2017; He et al., 2021; Ma
650 et al., 2019). Therefore, ACDC_RM_SF0.5 exhibits consistent applicability as other
651 two parameterizations at around ~ 280 K. However, attributed to an inappropriate
652 representation of cluster thermodynamics, ACDC_RM_SF0.5 has limitations in
653 predicting particle formation rates at elevated temperatures. Overall, considering all
654 aspects, we recommend ACDC_DB as a more reliable parameterization for simulating
655 NPF across various atmospheric environments.

656 In addition to contributing to a more reasonable 3-D modeling of NPF, our research
657 further provides valuable references for the development of parameterizations for other
658 nucleation systems. Firstly, we demonstrate the efficacy of the DLPNO-CCSD(T)/aug-



659 cc-pVTZ// ω B97X-D/6-311++G(3df,3pd) level of theory in describing the
660 thermodynamic properties of SA-DMA clusters through comprehensive evidence. This
661 approach can thus be referenced when using quantum chemical calculations to obtain
662 thermodynamic data for other nucleation clusters, especially for other alkylamines such
663 as methylamine/trimethylamine-sulfuric acid clusters. It should be also noted, however,
664 that in some qualitative studies, e.g., comparing the enhancing potential or synergistic
665 effects of different precursors in SA-driven nucleation, methods other than DLPNO-
666 CCSD(T)/aug-cc-pVTZ// ω B97X-D/6-311++G(3df,3pd), such as RI-CC2/aug-cc-
667 pV(T+d)Z//M06-2X/6-311++G(3df,3pd), are equally valid (Liu et al., 2019). Secondly,
668 we provide comprehensive modeling evidences that certain simplifications or
669 assumptions in cluster dynamics, such as reducing the number of expected clusters,
670 modifying boundary conditions, and assuming certain clusters to be non-evaporative,
671 can significantly impact the prediction of particle formation rates and hence alter the 3-
672 D NPF simulation under certain conditions. While applying certain simplifications
673 concurrently under specific ambient conditions can offset different influences against
674 each other, leading to a satisfactory model-observation comparison, there is a risk that
675 certain simplifications may drive the model's outcomes away from reality when
676 environmental conditions change. Therefore, caution should be exercised when
677 applying these simplifications in derivation of nucleation parameterizations and
678 subsequent application in 3-D models. Lastly, we note that the development of cluster
679 dynamics-based nucleation parameterizations in the form of explicit mathematical
680 expressions is subject to limitations, especially for systems involving multiple
681 precursor species (Semeniuk and Dastoor, 2018). Given that the original ACDC has
682 been extended to involve more than two precursor species, the ACDC-derived
683 parameterization framework, in the form of a look-up table, is highly meaningful for
684 establishing parameterizations for these multi-component nucleation systems.
685



686 **Appendix.** Abbreviations used in the main text.

687

688 **SA:** sulfuric acid

689 **DMA:** dimethylamine

690 **ACDC:** Atmospheric Cluster Dynamic Code

691 **DB:** DLPNO-CCSD(T)/aug-cc-pVTZ// ω B97X-D/6-311++G(3df,3pd) level of theory

692 **RM:** RI-CC2/aug-cc-pV(T+d)Z//M06-2X/6-311++G(3df,3pd) level of theory

693 **CE:** simplification in cluster evaporations (only $(SA)_k(DMA)_k$ ($k = 1-4$) and
694 $(SA)_2(DMA)_1$ clusters are considered)

695 **CN:** simplification in cluster number (clusters larger than $(SA)_1(DMA)_1$ are regarded
696 stable with no evaporation)

697 **BC:** simplification in boundary conditions ($(SA)_4(DMA)_4$ cluster is set as the only
698 terminal cluster in calculating particle formation rates)

699 **SF:** sticking factor used in collision process

700 **Dynamic_Sim:** a reported cluster-dynamic based parameterization incorporating
701 simplifications of CE, CN and BC.

702 **$J_{1.4}$:** particle formation rate at 1.4 nm

703 **R :** a parameter to quantify the differences in simulating $J_{1.4}$ among different cluster
704 dynamics-based parameterizations compared to the base-case ACDC_DB

705



706 **Code and data availability.** The data and code used in this study are available upon
707 request from the corresponding author.

708

709 **Author contributions.** JS, BZ, and SW designed the research; AN and XZ collected
710 the quantum chemistry calculation data; JS performed the ACDC and WRF-
711 Chem/R2D-VBS simulations; YL, RC, and JJ collected the observational data. JS, BZ,
712 and SW analyzed the data; RC, DG, JJ, YG, MS, BC, and HH presented important
713 suggestions for the paper; JS, BZ, and SW wrote the paper with input from all co-
714 authors.

715

716 **Competing interests.** At least one of the (co-)authors is a member of the editorial board
717 of Atmospheric Chemistry and Physics.

718

719 **Acknowledgements.** This study was supported by the National Natural Science
720 Foundation of China (22188102 and 42275110).

721

722 **Financial support.** Financial support from National Natural Science Foundation of
723 China (22188102 and 42275110).

724

725



726 **REFERENCES**

- 727 Almeida, J., Schobesberger, S., Kurten, A., Ortega, I. K., Kupiainen-Maatta, O.,
728 Praplan, A. P., Adamov, A., Amorim, A., Bianchi, F., Breitenlechner, M.,
729 David, A., Dommen, J., Donahue, N. M., Downard, A., Dunne, E., Duplissy,
730 J., Ehrhart, S., Flagan, R. C., Franchin, A., Guida, R., Hakala, J., Hansel, A.,
731 Heinritzi, M., Henschel, H., Jokinen, T., Junninen, H., Kajos, M.,
732 Kangasluoma, J., Keskinen, H., Kupc, A., Kurten, T., Kvashin, A. N.,
733 Laaksonen, A., Lehtipalo, K., Leiminger, M., Leppa, J., Loukonen, V.,
734 Makhmutov, V., Mathot, S., McGrath, M. J., Nieminen, T., Olenius, T.,
735 Onnela, A., Petaja, T., Riccobono, F., Riipinen, I., Rissanen, M., Rondo, L.,
736 Ruuskanen, T., Santos, F. D., Sarnela, N., Schallhart, S., Schnitzhofer, R.,
737 Seinfeld, J. H., Simon, M., Sipila, M., Stozhkov, Y., Stratmann, F., Tome, A.,
738 Trostl, J., Tsagkogeorgas, G., Vaattovaara, P., Viisanen, Y., Virtanen, A., Vrtala,
739 A., Wagner, P. E., Weingartner, E., Wex, H., Williamson, C., Wimmer, D., Ye,
740 P., Yli-Juuti, T., Carslaw, K. S., Kulmala, M., Curtius, J., Baltensperger, U.,
741 Worsnop, D. R., Vehkamäki, H., and Kirkby, J.: Molecular understanding of
742 sulphuric acid-amine particle nucleation in the atmosphere, *Nature*, 502, 359-
743 363, 10.1038/nature12663, 2013.
- 744 Bergman, T., Laaksonen, A., Korhonen, H., Malila, J., Dunne, E. M., Mielonen, T.,
745 Lehtinen, K. E. J., Kühn, T., Arola, A., and Kokkola, H.: Geographical and
746 diurnal features of amine - enhanced boundary layer nucleation, *Journal of*
747 *Geophysical Research: Atmospheres*, 120, 9606-9624, 10.1002/2015jd023181,
748 2015.
- 749 Besel, V., Kubecka, J., Kurten, T., and Vehkamäki, H.: Impact of Quantum Chemistry
750 Parameter Choices and Cluster Distribution Model Settings on Modeled
751 Atmospheric Particle Formation Rates, *J Phys Chem A*, 124, 5931-5943,
752 10.1021/acs.jpca.0c03984, 2020.
- 753 Cai, R. and Jiang, J.: A new balance formula to estimate new particle formation rate:
754 reevaluating the effect of coagulation scavenging, *Atmospheric Chemistry and*
755 *Physics*, 17, 12659-12675, 10.5194/acp-17-12659-2017, 2017.
- 756 Cai, R., Yin, R., Li, X., Xie, H.-B., Yang, D., Kerminen, V.-M., Smith, J. N., Ma, Y.,
757 Hao, J., Chen, J., Kulmala, M., Zheng, J., Jiang, J., and Elm, J.: Significant
758 contributions of trimethylamine to sulfuric acid nucleation in polluted
759 environments, *npj Climate and Atmospheric Science*, 6, 10.1038/s41612-023-
760 00405-3, 2023.
- 761 Cai, R., Yan, C., Yang, D., Yin, R., Lu, Y., Deng, C., Fu, Y., Ruan, J., Li, X.,
762 Kontkanen, J., Zhang, Q., Kangasluoma, J., Ma, Y., Hao, J., Worsnop, D. R.,
763 Bianchi, F., Paasonen, P., Kerminen, V.-M., Liu, Y., Wang, L., Zheng, J.,
764 Kulmala, M., and Jiang, J.: Sulfuric acid-amine nucleation in urban Beijing,
765 *Atmospheric Chemistry and Physics*, 21, 2457-2468, 10.5194/acp-21-2457-
766 2021, 2021.
- 767 Chu, B., Kerminen, V.-M., Bianchi, F., Yan, C., Petäjä, T., and Kulmala, M.:



- 768 Atmospheric new particle formation in China, *Atmospheric Chemistry and*
769 *Physics*, 19, 115-138, 10.5194/acp-19-115-2019, 2019.
- 770 Dal Maso, M., Hyvärinen, A., Komppula, M., Tunved, P., Kerminen, V.-M.,
771 Lihavainen, H., Viisanen, Y., Hansson, H.-C., and Kulmala, M.: Annual and
772 interannual variation in boreal forest aerosol particle number and volume
773 concentration and their connection to particle formation, *Tellus B: Chemical*
774 *and Physical Meteorology*, 60, 10.1111/j.1600-0889.2008.00366.x, 2008.
- 775 Deng, C., Fu, Y., Dada, L., Yan, C., Cai, R., Yang, D., Zhou, Y., Yin, R., Lu, Y., Li, X.,
776 Qiao, X., Fan, X., Nie, W., Kontkanen, J., Kangasluoma, J., Chu, B., Ding, A.,
777 Kerminen, V. M., Paasonen, P., Worsnop, D. R., Bianchi, F., Liu, Y., Zheng, J.,
778 Wang, L., Kulmala, M., and Jiang, J.: Seasonal Characteristics of New Particle
779 Formation and Growth in Urban Beijing, *Environ Sci Technol*, 54, 8547-8557,
780 10.1021/acs.est.0c00808, 2020.
- 781 Dunne, E. M., Gordon, H., Kurten, A., Almeida, J., Duplissy, J., Williamson, C.,
782 Ortega, I. K., Pringle, K. J., Adamov, A., Baltensperger, U., Barmet, P.,
783 Benduhn, F., Bianchi, F., Breitenlechner, M., Clarke, A., Curtius, J., Dommen,
784 J., Donahue, N. M., Ehrhart, S., Flagan, R. C., Franchin, A., Guida, R.,
785 Hakala, J., Hansel, A., Heinritzi, M., Jokinen, T., Kangasluoma, J., Kirkby, J.,
786 Kulmala, M., Kupc, A., Lawler, M. J., Lehtipalo, K., Makhmutov, V., Mann,
787 G., Mathot, S., Merikanto, J., Miettinen, P., Nenes, A., Onnela, A., Rap, A.,
788 Reddington, C. L., Riccobono, F., Richards, N. A., Rissanen, M. P., Rondo, L.,
789 Sarnela, N., Schobesberger, S., Sengupta, K., Simon, M., Sipila, M., Smith, J.
790 N., Stozkhov, Y., Tome, A., Trostl, J., Wagner, P. E., Wimmer, D., Winkler, P.
791 M., Worsnop, D. R., and Carslaw, K. S.: Global atmospheric particle
792 formation from CERN CLOUD measurements, *Science*, 354, 1119-1124,
793 10.1126/science.aaf2649, 2016.
- 794 Elm, J., Bilde, M., and Mikkelsen, K. V.: Assessment of binding energies of
795 atmospherically relevant clusters, *Phys Chem Chem Phys*, 15, 16442-16445,
796 10.1039/c3cp52616j, 2013.
- 797 Elm, J., Kubečka, J., Besel, V., Jääskeläinen, M. J., Halonen, R., Kurtén, T., and
798 Vehkamäki, H.: Modeling the formation and growth of atmospheric molecular
799 clusters: A review, *Journal of Aerosol Science*, 149,
800 10.1016/j.jaerosci.2020.105621, 2020.
- 801 Gordon, H., Sengupta, K., Rap, A., Duplissy, J., Frege, C., Williamson, C., Heinritzi,
802 M., Simon, M., Yan, C., Almeida, J., Trostl, J., Nieminen, T., Ortega, I. K.,
803 Wagner, R., Dunne, E. M., Adamov, A., Amorim, A., Bernhammer, A. K.,
804 Bianchi, F., Breitenlechner, M., Brilke, S., Chen, X., Craven, J. S., Dias, A.,
805 Ehrhart, S., Fischer, L., Flagan, R. C., Franchin, A., Fuchs, C., Guida, R.,
806 Hakala, J., Hoyle, C. R., Jokinen, T., Junninen, H., Kangasluoma, J., Kim, J.,
807 Kirkby, J., Krapf, M., Kurten, A., Laaksonen, A., Lehtipalo, K., Makhmutov,
808 V., Mathot, S., Molteni, U., Monks, S. A., Onnela, A., Perakyla, O., Piel, F.,
809 Petaja, T., Praplan, A. P., Pringle, K. J., Richards, N. A., Rissanen, M. P.,



- 810 Rondo, L., Sarnela, N., Schobesberger, S., Scott, C. E., Seinfeld, J. H.,
811 Sharma, S., Sipila, M., Steiner, G., Stozhkov, Y., Stratmann, F., Tome, A.,
812 Virtanen, A., Vogel, A. L., Wagner, A. C., Wagner, P. E., Weingartner, E.,
813 Wimmer, D., Winkler, P. M., Ye, P., Zhang, X., Hansel, A., Dommen, J.,
814 Donahue, N. M., Worsnop, D. R., Baltensperger, U., Kulmala, M., Curtius, J.,
815 and Carslaw, K. S.: Reduced anthropogenic aerosol radiative forcing caused
816 by biogenic new particle formation, *Proc Natl Acad Sci U S A*, 113, 12053-
817 12058, 10.1073/pnas.1602360113, 2016.
- 818 Guenther, A., Karl, T., Harley, P., Wiedinmyer, C., Palmer, P. I., and Geron, C.:
819 Estimates of global terrestrial isoprene emissions using MEGAN (Model of
820 Emissions of Gases and Aerosols from Nature), *Atmos. Chem. Phys.*, 6, 3181-
821 3210, 10.5194/acp-6-3181-2006, 2006.
- 822 He, X. C., Tham, Y. J., Dada, L., Wang, M., Finkenzeller, H., Stolzenburg, D., Iyer, S.,
823 Simon, M., Kurten, A., Shen, J., Rorup, B., Rissanen, M., Schobesberger, S.,
824 Baalbaki, R., Wang, D. S., Koenig, T. K., Jokinen, T., Sarnela, N., Beck, L. J.,
825 Almeida, J., Amanatidis, S., Amorim, A., Ataei, F., Baccharini, A., Bertozzi, B.,
826 Bianchi, F., Brilke, S., Caudillo, L., Chen, D., Chiu, R., Chu, B., Dias, A.,
827 Ding, A., Dommen, J., Duplissy, J., El Haddad, I., Gonzalez Carracedo, L.,
828 Granzin, M., Hansel, A., Heinritzi, M., Hofbauer, V., Junninen, H.,
829 Kangasluoma, J., Kempainen, D., Kim, C., Kong, W., Krechmer, J. E.,
830 Kvashin, A., Laitinen, T., Lamkaddam, H., Lee, C. P., Lehtipalo, K.,
831 Leiminger, M., Li, Z., Makhmutov, V., Manninen, H. E., Marie, G., Marten,
832 R., Mathot, S., Mauldin, R. L., Mentler, B., Mohler, O., Muller, T., Nie, W.,
833 Onnela, A., Petaja, T., Pfeifer, J., Philippov, M., Ranjithkumar, A., Saiz-Lopez,
834 A., Salma, I., Scholz, W., Schuchmann, S., Schulze, B., Steiner, G., Stozhkov,
835 Y., Tauber, C., Tome, A., Thakur, R. C., Vaisanen, O., Vazquez-Pufleau, M.,
836 Wagner, A. C., Wang, Y., Weber, S. K., Winkler, P. M., Wu, Y., Xiao, M., Yan,
837 C., Ye, Q., Ylisirnio, A., Zauner-Wieczorek, M., Zha, Q., Zhou, P., Flagan, R.
838 C., Curtius, J., Baltensperger, U., Kulmala, M., Kerminen, V. M., Kurten, T.,
839 Donahue, N. M., Volkamer, R., Kirkby, J., Worsnop, D. R., and Sipila, M.:
840 Role of iodine oxoacids in atmospheric aerosol nucleation, *Science*, 371, 589-
841 595, 10.1126/science.abe0298, 2021.
- 842 Jen, C. N., Hanson, D. R., and McMurry, P. H.: Toward Reconciling Measurements of
843 Atmospherically Relevant Clusters by Chemical Ionization Mass
844 Spectrometry and Mobility Classification/Vapor Condensation, *Aerosol
845 Science and Technology*, 49, i-iii, 10.1080/02786826.2014.1002602, 2014.
- 846 Kirkby, J., Curtius, J., Almeida, J., Dunne, E., Duplissy, J., Ehrhart, S., Franchin, A.,
847 Gagne, S., Ickes, L., Kurten, A., Kupc, A., Metzger, A., Riccobono, F., Rondo,
848 L., Schobesberger, S., Tsagkogeorgas, G., Wimmer, D., Amorim, A., Bianchi,
849 F., Breitenlechner, M., David, A., Dommen, J., Downard, A., Ehn, M., Flagan,
850 R. C., Haider, S., Hansel, A., Hauser, D., Jud, W., Junninen, H., Kreissl, F.,
851 Kvashin, A., Laaksonen, A., Lehtipalo, K., Lima, J., Lovejoy, E. R.,



- 852 Makhmutov, V., Mathot, S., Mikkilä, J., Minginette, P., Mogo, S., Nieminen,
853 T., Onnela, A., Pereira, P., Petaja, T., Schnitzhofer, R., Seinfeld, J. H., Sipila,
854 M., Stozhkov, Y., Stratmann, F., Tome, A., Vanhanen, J., Viisanen, Y., Vrtala,
855 A., Wagner, P. E., Walther, H., Weingartner, E., Wex, H., Winkler, P. M.,
856 Carslaw, K. S., Worsnop, D. R., Baltensperger, U., and Kulmala, M.: Role of
857 sulphuric acid, ammonia and galactic cosmic rays in atmospheric aerosol
858 nucleation, *Nature*, 476, 429-433, 10.1038/nature10343, 2011.
- 859 Kirkby, J., Duplissy, J., Sengupta, K., Frege, C., Gordon, H., Williamson, C.,
860 Heinritzi, M., Simon, M., Yan, C., Almeida, J., Trostl, J., Nieminen, T., Ortega,
861 I. K., Wagner, R., Adamov, A., Amorim, A., Bernhammer, A. K., Bianchi, F.,
862 Breitenlechner, M., Brilke, S., Chen, X., Craven, J., Dias, A., Ehrhart, S.,
863 Flagan, R. C., Franchin, A., Fuchs, C., Guida, R., Hakala, J., Hoyle, C. R.,
864 Jokinen, T., Junninen, H., Kangasluoma, J., Kim, J., Krapf, M., Kurten, A.,
865 Laaksonen, A., Lehtipalo, K., Makhmutov, V., Mathot, S., Molteni, U.,
866 Onnela, A., Perakyla, O., Piel, F., Petaja, T., Praplan, A. P., Pringle, K., Rap,
867 A., Richards, N. A., Riipinen, I., Rissanen, M. P., Rondo, L., Sarnela, N.,
868 Schobesberger, S., Scott, C. E., Seinfeld, J. H., Sipila, M., Steiner, G.,
869 Stozhkov, Y., Stratmann, F., Tome, A., Virtanen, A., Vogel, A. L., Wagner, A.
870 C., Wagner, P. E., Weingartner, E., Wimmer, D., Winkler, P. M., Ye, P., Zhang,
871 X., Hansel, A., Dommen, J., Donahue, N. M., Worsnop, D. R., Baltensperger,
872 U., Kulmala, M., Carslaw, K. S., and Curtius, J.: Ion-induced nucleation of
873 pure biogenic particles, *Nature*, 533, 521-526, 10.1038/nature17953, 2016.
- 874 Kulmala, M., Lehtinen, K. E. J., and Laaksonen, A.: Cluster activation theory as an
875 explanation of the linear dependence between formation rate of 3nm particles
876 and sulphuric acid concentration, *Atmospheric Chemistry and Physics*, 6, 787-
877 793, DOI 10.5194/acp-6-787-2006, 2006.
- 878 Kürten, A., Li, C., Bianchi, F., Curtius, J., Dias, A., Donahue, N. M., Duplissy, J.,
879 Flagan, R. C., Hakala, J., Jokinen, T., Kirkby, J., Kulmala, M., Laaksonen, A.,
880 Lehtipalo, K., Makhmutov, V., Onnela, A., Rissanen, M. P., Simon, M., Sipilä,
881 M., Stozhkov, Y., Tröstl, J., Ye, P., and McMurry, P. H.: New particle
882 formation in the sulfuric acid–dimethylamine–water system: reevaluation of
883 CLOUD chamber measurements and comparison to an aerosol nucleation and
884 growth model, *Atmospheric Chemistry and Physics*, 18, 845-863,
885 10.5194/acp-18-845-2018, 2018.
- 886 Lehtinen, K. E. J., Dal Maso, M., Kulmala, M., and Kerminen, V. M.: Estimating
887 nucleation rates from apparent particle formation rates and vice versa: Revised
888 formulation of the Kerminen-Kulmala equation, *Journal of Aerosol Science*,
889 38, 988-994, 10.1016/j.jaerosci.2007.06.009, 2007.
- 890 Li, C., Zhao, Y., Li, Z., Liu, L., Zhang, X., Zheng, J., Kerminen, V.-M., Kulmala, M.,
891 Jiang, J., Cai, R., and Xiao, H.: The dependence of new particle formation
892 rates on the interaction between cluster growth, evaporation, and condensation
893 sink, *Environmental Science: Atmospheres*, 3, 168-181, 10.1039/d2ea00066k,



- 894 2023a.
- 895 Li, H., Ning, A., Zhong, J., Zhang, H., Liu, L., Zhang, Y., Zhang, X., Zeng, X. C., and
896 He, H.: Influence of atmospheric conditions on sulfuric acid-dimethylamine-
897 ammonia-based new particle formation, *Chemosphere*, 245, 125554,
898 10.1016/j.chemosphere.2019.125554, 2020.
- 899 Li, M., Zhang, Q., Kurokawa, J., Woo, J. H., He, K. B., Lu, Z. F., Ohara, T., Song, Y.,
900 Streets, D. G., Carmichael, G. R., Cheng, Y. F., Hong, C. P., Huo, H., Jiang, X.
901 J., Kang, S. C., Liu, F., Su, H., and Zheng, B.: MIX: a mosaic Asian
902 anthropogenic emission inventory under the international collaboration
903 framework of the MICS-Asia and HTAP, *Atmospheric Chemistry and Physics*,
904 17, 935-963, 10.5194/acp-17-935-2017, 2017.
- 905 Li, S., Wang, S., Wu, Q., Zhang, Y., Ouyang, D., Zheng, H., Han, L., Qiu, X., Wen, Y.,
906 Liu, M., Jiang, Y., Yin, D., Liu, K., Zhao, B., Zhang, S., Wu, Y., and Hao, J.:
907 Emission trends of air pollutants and CO₂ in China from 2005 to 2021, *Earth
908 System Science Data*, 15, 2279-2294, 10.5194/essd-15-2279-2023, 2023b.
- 909 Li, Y., Shen, J., Zhao, B., Cai, R., Wang, S., Gao, Y., Shrivastava, M., Gao, D., Zheng,
910 J., Kulmala, M., and Jiang, J.: A dynamic parameterization of sulfuric acid-
911 dimethylamine nucleation and its application in three-dimensional modeling,
912 *Atmospheric Chemistry and Physics*, 23, 8789-8804, 10.5194/acp-23-8789-
913 2023, 2023c.
- 914 Liu, L., Yu, F., Tu, K., Yang, Z., and Zhang, X.: Influence of atmospheric conditions
915 on the role of trifluoroacetic acid in atmospheric sulfuric acid-dimethylamine
916 nucleation, *Atmospheric Chemistry and Physics*, 21, 6221-6230, 10.5194/acp-
917 21-6221-2021, 2021.
- 918 Liu, L., Zhong, J., Vehkamäki, H., Kurten, T., Du, L., Zhang, X., Francisco, J. S., and
919 Zeng, X. C.: Unexpected quenching effect on new particle formation from the
920 atmospheric reaction of methanol with SO₃, *Proc Natl Acad Sci U S A*, 116,
921 24966-24971, 10.1073/pnas.1915459116, 2019.
- 922 Lu, Y., Liu, L., Ning, A., Yang, G., Liu, Y., Kurtén, T., Vehkamäki, H., Zhang, X., and
923 Wang, L.: Atmospheric Sulfuric Acid - Dimethylamine Nucleation Enhanced
924 by Trifluoroacetic Acid, *Geophysical Research Letters*, 47,
925 10.1029/2019gl085627, 2020.
- 926 Ma, F., Xie, H. B., Elm, J., Shen, J., Chen, J., and Vehkamäki, H.: Piperazine
927 Enhancing Sulfuric Acid-Based New Particle Formation: Implications for the
928 Atmospheric Fate of Piperazine, *Environ Sci Technol*, 53, 8785-8795,
929 10.1021/acs.est.9b02117, 2019.
- 930 McGrath, M. J., Olenius, T., Ortega, I. K., Loukonen, V., Paasonen, P., Kurtén, T.,
931 Kulmala, M., and Vehkamäki, H.: Atmospheric Cluster Dynamics Code: a
932 flexible method for solution of the birth-death equations, *Atmospheric
933 Chemistry and Physics*, 12, 2345-2355, 10.5194/acp-12-2345-2012, 2012.
- 934 Myllys, N., Chee, S., Olenius, T., Lawler, M., and Smith, J.: Molecular-Level
935 Understanding of Synergistic Effects in Sulfuric Acid-Amine-Ammonia



- 936 Mixed Clusters, *J Phys Chem A*, 123, 2420-2425, 10.1021/acs.jpca.9b00909,
937 2019.
- 938 Ning, A. and Zhang, X.: The synergistic effects of methanesulfonic acid (MSA) and
939 methanesulfonic acid (MSIA) on marine new particle formation, *Atmospheric*
940 *Environment*, 269, 10.1016/j.atmosenv.2021.118826, 2022.
- 941 Ning, A., Liu, L., Ji, L., and Zhang, X.: Molecular-level nucleation mechanism of
942 iodic acid and methanesulfonic acid, *Atmospheric Chemistry and Physics*, 22,
943 6103-6114, 10.5194/acp-22-6103-2022, 2022.
- 944 Ning, A., Zhang, H., Zhang, X., Li, Z., Zhang, Y., Xu, Y., and Ge, M.: A molecular-
945 scale study on the role of methanesulfonic acid in marine new particle
946 formation, *Atmospheric Environment*, 227, 10.1016/j.atmosenv.2020.117378,
947 2020.
- 948 Ning, A., Shen, J., Zhao, B., Wang, S., Cai, R., Jiang, J. Yan, C., Fu, X., Zhang, Y., Li,
949 J., Ouyang, D., Sun, Y., Saiz-Lopez, A., Francisco, J., and Zhang, X.:
950 Overlooked significance of iodic acid in new particle formation in the
951 continental atmosphere, 2024. In Preparation.
- 952 Ortega, I. K., Kupiainen, O., Kurtén, T., Olenius, T., Wilkman, O., McGrath, M. J.,
953 Loukonen, V., and Vehkamäki, H.: From quantum chemical formation free
954 energies to evaporation rates, *Atmospheric Chemistry and Physics*, 12, 225-
955 235, 10.5194/acp-12-225-2012, 2012.
- 956 Riccobono, F., Schobesberger, S., Scott, C. E., Dommen, J., Ortega, I. K., Rondo, L.,
957 Almeida, J., Amorim, A., Bianchi, F., Breitenlechner, M., David, A., Downard,
958 A., Dunne, E. M., Duplissy, J., Ehrhart, S., Flagan, R. C., Franchin, A.,
959 Hansel, A., Junninen, H., Kajos, M., Keskinen, H., Kupc, A., Kurten, A.,
960 Kvashin, A. N., Laaksonen, A., Lehtipalo, K., Makhmutov, V., Mathot, S.,
961 Nieminen, T., Onnela, A., Petaja, T., Praplan, A. P., Santos, F. D., Schallhart,
962 S., Seinfeld, J. H., Sipila, M., Spracklen, D. V., Stozhkov, Y., Stratmann, F.,
963 Tome, A., Tsagkogeorgas, G., Vaattovaara, P., Viisanen, Y., Vrtala, A., Wagner,
964 P. E., Weingartner, E., Wex, H., Wimmer, D., Carslaw, K. S., Curtius, J.,
965 Donahue, N. M., Kirkby, J., Kulmala, M., Worsnop, D. R., and Baltensperger,
966 U.: Oxidation Products of Biogenic Emissions Contribute to Nucleation of
967 Atmospheric Particles, *Science*, 344, 717-721, 10.1126/science.1243527,
968 2014.
- 969 Semeniuk, K. and Dastoor, A.: Current state of aerosol nucleation parameterizations
970 for air-quality and climate modeling, *Atmospheric Environment*, 179, 77-106,
971 10.1016/j.atmosenv.2018.01.039, 2018.
- 972 Stolzenburg, D., Simon, M., Ranjithkumar, A., Kürten, A., Lehtipalo, K., Gordon, H.,
973 Ehrhart, S., Finkenzeller, H., Pichelstorfer, L., Nieminen, T., He, X.-C., Brilke,
974 S., Xiao, M., Amorim, A., Baalbaki, R., Baccharini, A., Beck, L., Bräkling, S.,
975 Caudillo Murillo, L., Chen, D., Chu, B., Dada, L., Dias, A., Dommen, J.,
976 Duplissy, J., El Haddad, I., Fischer, L., Gonzalez Carracedo, L., Heinritzi, M.,
977 Kim, C., Koenig, T. K., Kong, W., Lamkaddam, H., Lee, C. P., Leiminger, M.,



- 978 Li, Z., Makhmutov, V., Manninen, H. E., Marie, G., Marten, R., Müller, T.,
979 Nie, W., Partoll, E., Petäjä, T., Pfeifer, J., Philippov, M., Rissanen, M. P.,
980 Rörup, B., Schobesberger, S., Schuchmann, S., Shen, J., Sipilä, M., Steiner,
981 G., Stozhkov, Y., Tauber, C., Tham, Y. J., Tomé, A., Vazquez-Pufleau, M.,
982 Wagner, A. C., Wang, M., Wang, Y., Weber, S. K., Wimmer, D., Wlasits, P. J.,
983 Wu, Y., Ye, Q., Zauner-Wieczorek, M., Baltensperger, U., Carslaw, K. S.,
984 Curtius, J., Donahue, N. M., Flagan, R. C., Hansel, A., Kulmala, M.,
985 Lelieveld, J., Volkamer, R., Kirkby, J., and Winkler, P. M.: Enhanced growth
986 rate of atmospheric particles from sulfuric acid, *Atmospheric Chemistry and*
987 *Physics*, 20, 7359-7372, 10.5194/acp-20-7359-2020, 2020.
- 988 Thomas, J. M., He, S., Larriba-Andaluz, C., DePalma, J. W., Johnston, M. V., and
989 Hogan, C. J., Jr.: Ion mobility spectrometry-mass spectrometry examination of
990 the structures, stabilities, and extents of hydration of dimethylamine-sulfuric
991 acid clusters, *Phys Chem Chem Phys*, 18, 22962-22972, 10.1039/c6cp03432b,
992 2016.
- 993 Xiao, M., Hoyle, C. R., Dada, L., Stolzenburg, D., Kürten, A., Wang, M.,
994 Lamkaddam, H., Garmash, O., Mentler, B., Molteni, U., Baccarini, A., Simon,
995 M., He, X.-C., Lehtipalo, K., Ahonen, L. R., Baalbaki, R., Bauer, P. S., Beck,
996 L., Bell, D., Bianchi, F., Brilke, S., Chen, D., Chiu, R., Dias, A., Duplissy, J.,
997 Finkenzeller, H., Gordon, H., Hofbauer, V., Kim, C., Koenig, T. K.,
998 Lampilahti, J., Lee, C. P., Li, Z., Mai, H., Makhmutov, V., Manninen, H. E.,
999 Marten, R., Mathot, S., Mauldin, R. L., Nie, W., Onnela, A., Partoll, E., Petäjä,
1000 T., Pfeifer, J., Pospisilova, V., Quéléver, L. L. J., Rissanen, M., Schobesberger,
1001 S., Schuchmann, S., Stozhkov, Y., Tauber, C., Tham, Y. J., Tomé, A., Vazquez-
1002 Pufleau, M., Wagner, A. C., Wagner, R., Wang, Y., Weitz, L., Wimmer, D., Wu,
1003 Y., Yan, C., Ye, P., Ye, Q., Zha, Q., Zhou, X., Amorim, A., Carslaw, K.,
1004 Curtius, J., Hansel, A., Volkamer, R., Winkler, P. M., Flagan, R. C., Kulmala,
1005 M., Worsnop, D. R., Kirkby, J., Donahue, N. M., Baltensperger, U., El
1006 Haddad, I., and Dommen, J.: The driving factors of new particle formation and
1007 growth in the polluted boundary layer, *Atmospheric Chemistry and Physics*,
1008 21, 14275-14291, 10.5194/acp-21-14275-2021, 2021.
- 1009 Xie, H. B., Elm, J., Halonen, R., Myllys, N., Kurten, T., Kulmala, M., and Vehkamäki,
1010 H.: Atmospheric Fate of Monoethanolamine: Enhancing New Particle
1011 Formation of Sulfuric Acid as an Important Removal Process, *Environ Sci*
1012 *Technol*, 51, 8422-8431, 10.1021/acs.est.7b02294, 2017.
- 1013 Yang, S., Liu, Z., Clusius, P. S., Liu, Y., Zou, J., Yang, Y., Zhao, S., Zhang, G., Xu, Z.,
1014 Ma, Z., Yang, Y., Sun, J., Pan, Y., Ji, D., Hu, B., Yan, C., Boy, M., Kulmala,
1015 M., and Wang, Y.: Chemistry of new particle formation and growth events
1016 during wintertime in suburban area of Beijing: Insights from highly polluted
1017 atmosphere, *Atmospheric Research*, 255, 10.1016/j.atmosres.2021.105553,
1018 2021.
- 1019 Yao, L., Garmash, O., Bianchi, F., Zheng, J., Yan, C., Kontkanen, J., Junninen, H.,



- 1020 Mazon, S. B., Ehn, M., Paasonen, P., Sipila, M., Wang, M., Wang, X., Xiao,
1021 S., Chen, H., Lu, Y., Zhang, B., Wang, D., Fu, Q., Geng, F., Li, L., Wang, H.,
1022 Qiao, L., Yang, X., Chen, J., Kerminen, V. M., Petaja, T., Worsnop, D. R.,
1023 Kulmala, M., and Wang, L.: Atmospheric new particle formation from sulfuric
1024 acid and amines in a Chinese megacity, *Science*, 361, 278-281,
1025 10.1126/science.aao4839, 2018.
- 1026 Yu, F.: Ion-mediated nucleation in the atmosphere: Key controlling parameters,
1027 implications, and look-up table, *Journal of Geophysical Research*, 115,
1028 10.1029/2009jd012630, 2010.
- 1029 Zhao, B., Shrivastava, M., Donahue, N. M., Gordon, H., Schervish, M., Shilling, J. E.,
1030 Zaveri, R. A., Wang, J., Andreae, M. O., Zhao, C., Gaudet, B., Liu, Y., Fan, J.,
1031 and Fast, J. D.: High concentration of ultrafine particles in the Amazon free
1032 troposphere produced by organic new particle formation, *Proc Natl Acad Sci*
1033 *U S A*, 117, 25344-25351, 10.1073/pnas.2006716117, 2020.
- 1034 Zheng, H. T., Cai, S. Y., Wang, S. X., Zhao, B., Chang, X., and Hao, J. M.:
1035 Development of a unit-based industrial emission inventory in the Beijing-
1036 Tianjin-Hebei region and resulting improvement in air quality modeling,
1037 *Atmospheric Chemistry and Physics*, 19, 3447-3462, 10.5194/acp-19-3447-
1038 2019, 2019.
- 1039